Structural description of surfaces and interfaces in biominerals by DNP SENS

Thierry Azais, Stanislas von Euw, Widad Ajili, Stéphanie Auzoux-Bordenave, Philippe Bertani, David Gajan, Lyndon Emsley, Nadine Nassif, Anne Lesage

Structural description of surfaces and interfaces in biominerals by DNP SENS

Thierry Azaïs[a]*, Stanislas Von Euw,[a] Widad Ajili,[a] Stéphanie Auzoux-Bordenave,[b] Philippe Bertani,[c] David Gajan,[d] Lyndon Emsley,[e] Nadine Nassif[a] and Anne Lesage[d]

[a] *Sorbonne Universités, CNRS, Collège de France, Laboratoire Chimie de la Matière Condensée de Paris (LCMCP), 4 place Jussieu F-75005 Paris, France*

[b] *Sorbonne Université, UMR BOREA, Biologie des Organismes et Ecosystèmes Aquatiques, MNHN/CNRS-7208/IRD-207/UPMC, Muséum National d'Histoire Naturelle, Station Marine de Concarneau, Place de la Croix 29900 Concarneau.*

[c] *Laboratoire de RMN et Biophysique des Membranes, UMR 7177 Chimie Université de Strasbourg, Institut Le Bel, 4 rue Blaise Pascal, 67008 Strasbourg*

[d] *High Field NMR Center of Lyon, CRNS/ENS Lyon/ UCB Lyon, 5 rue de la Doua, 69100 Villeurbanne, France*

[e] *Institut des Sciences et Ingénierie Chimiques, Ecole Polytechnique Fédérale de Lausanne (EPFL), CH-1015 Lausanne, Switzerland [d] Strasbourg*

** corresponding author : thierry.azais@upmc.fr*

Abstract

Biological mineralized tissues are hybrid materials with complex hierarchical architecture composed of biominerals often embedded in an organic matrix. The atomic-scale comprehension of surfaces and organo-mineral interfaces of these biominerals is of paramount importance to understand the ultrastructure, the formation mechanisms as well as the biological functions of the related biomineralized tissue. In this communication we demonstrate the capability of DNP SENS to reveal the fine atomic structure of biominerals, and more specifically their surfaces and interfaces. For this purpose, we studied two key examples belonging to the most significant biominerals family in nature: apatite in bone and aragonite in nacreous shell. As a result, we demonstrate that DNP SENS is a powerful approach for the study of intact biomineralized tissues. Signal enhancement factors are found to be up to 40 and 100, for the organic and the inorganic fractions, respectively, as soon as impregnation time with the radical solution is long enough (between 12 and 24 h) to allow an efficient radical penetration into the calcified tissues. Moreover, ions located at the biomineral surface are readily detected and identified through ^{31}P or ^{13}C HETCOR DNP SENS experiments. Noticeably, we show that protonated anions are preponderant at the biomineral surfaces that are in the form of HPO_4^{2-} for bone apatite and HCO_3^{2-} for nacreous aragonite. Finally, we demonstrate that organo-mineral interactions can be probed at the atomic level with high sensitivity. In particular, reliable $\{^{31}P\}$-^{13}C REDOR experiments are achieved in a few hours, leading to the determination of distances, molar proportion and binding mode of citrate bonded to bone mineral in native compact bone. According to our results, only 50% of the total amount of citrate in bone is directly interacting with bone apatite through two out of three carboxylic groups.

Keywords: Biomineralization, calcified tissues, biominerals, bone, nacre, solid state NMR, DNP SENS

Introduction

Biomineralization is the process by which living organisms produce minerals in order to protect or stiffen their tissues, for instance. Many biominerals of different chemical composition are found in nature. About 60 different biominerals have been described so far.[1] Two main families are particularly abundant in nature, namely calcium phosphates and calcium carbonates. The first group is mostly found in vertebrates in the form of hydroxyapatite (like in bones or teeth of mammalians), whereas the second is found in invertebrates in the form of calcite or aragonite (like in the shell of mollusks or gastropods along with the skeleton of stony corals).

Biominerals are usually closely associated to an organic matrix made of biological fibrous macromolecules (such as proteins or polysaccharides) in order to form functional mineralized tissues. Each biomineral possesses specific characteristics linked to the functions of the mineralized tissue in which it is embedded. Among these features one can cite (*i*) the chemical composition, (*ii*) the crystallographic structure, (*iii*) the size and the morphology of the crystals, (*iv*) the three-dimensional distribution within the organic matrix. The atomic-scale structural description of biominerals in mineralized tissue is thus crucial to understand the corresponding *in vivo* functions (mechanical or optical properties, role in metabolism...) as well as their underlying formation mechanism. Whereas numerous studies have been undertaken over years to understand the detailed structure of biominerals,[2,3,4] questions still remain open, in particular regarding the composition and organization at their surfaces and interfaces. It is now recognized that a distinct mineral domain exists around the crystalline core of biominerals in different calcified tissues such as bone,[5] dentin[6] or nacre.[7] This surface domain is described as amorphous or at least highly disordered. In the case of bone apatite, this surface domain is proposed to be involved *in vivo* in the structuration of platelets through a specific interaction with water molecules.[8] Nevertheless, a fine structural description is still lacking. This prevents a detailed understanding of the organo-mineral interface between the mineral phase and the extracellular matrix that is known to direct the nucleation, the growth, the morphology, the size and the 3D repartition of biominerals *in vivo*.

Solid-state NMR is in principle the method of choice to access a fine description of biomineralized tissues.[9,10,11] The intrinsic low sensitivity of this spectroscopy limits however its applicability to the investigation of surfaces and interfaces in materials of low specific surface area where the selective observation of surface *versus* bulk species is extremely challenging. In that context, Dynamic Nuclear Polarization (DNP) has recently emerged as an appealing technique to drastically enhance the sensitivity of solid-state NMR spectroscopy and, in particular, to amplify signals at surfaces in an approach called DNP SENS (DNP Surface Enhanced NMR Spectroscopy).[12] In a DNP experiment, the material is typically doped with unpaired electrons that act as a polarization source. These unpaired electrons are usually free radicals or metal ions. Upon microwave irradiation, the high electron spin polarization is transferred to neighboring nuclear spins either directly or by relayed mechanisms, resulting in signal enhancements by up to two orders of magnitude. One key approach to obtain high enhancement factors in intrinsically radical free materials is the use of incipient wetness impregnation,[13,14] which consists in wetting the powdered materials by a minimal amount of radical containing solution. Binitroxides radicals like AMUPOL[15] in aqueous solutions or TEKPOL[16] in organic solvents are today the most commonly employed polarizing agents but others are regularly introduced.[17] Recently, it was demonstrated that their design can be computationally assisted.[18] If the first proofs of concepts were reported on model mesoporous silica matrices of high

surface area, recent applications of DNP SENS concern a large range of chemical systems such as high performance organometallic heterogeneous catalysts, doped silicon surfaces, metal-organic frameworks, ligand-capped nanoparticles, cementitious materials, quantum dots or active Sn-zeolites.[19]

A few studies have been reported in the context of biomineralization. DNP SENS has thus been applied to investigate native bone tissue samples (cortical goat bone) by Sinha and co-workers, where imino acid-aromatic interactions within the collagen matrix were demonstrated.[20] In parallel, synthetic hydroxyapatite nanoparticles were studied by DNP enhanced ^{43}Ca and ^{13}C NMR experiments, providing new insights into the Ca^{2+} surface species[21] and the structural organization of bulk CO_3^{2-} substituted ions.[22]

In this communication we investigate the contribution of DNP SENS to the comprehension of surfaces and organo-mineral interfaces in natural biominerals through the study of two key examples belonging to the calcium phosphate and calcium carbonate families: bone apatite and aragonite from nacreous shells (**Fig. 1**). We show that DNP SENS performs extremely well on these materials, with signal enhancement factors of up to 100. Notably, surface ions could be readily observed and their nature revealed as hydrogen phosphates in bone apatite and as bicarbonates in nacre aragonite. Moreover, we demonstrate that organo-mineral interactions can be probed at the atomic level with high sensitivity. In particular reliable $\{^{31}P\}$-^{13}C REDOR experiments can be recorded in a few hours, leading to the determination of quantitative distances between citrate and bone mineral in native compact bone.

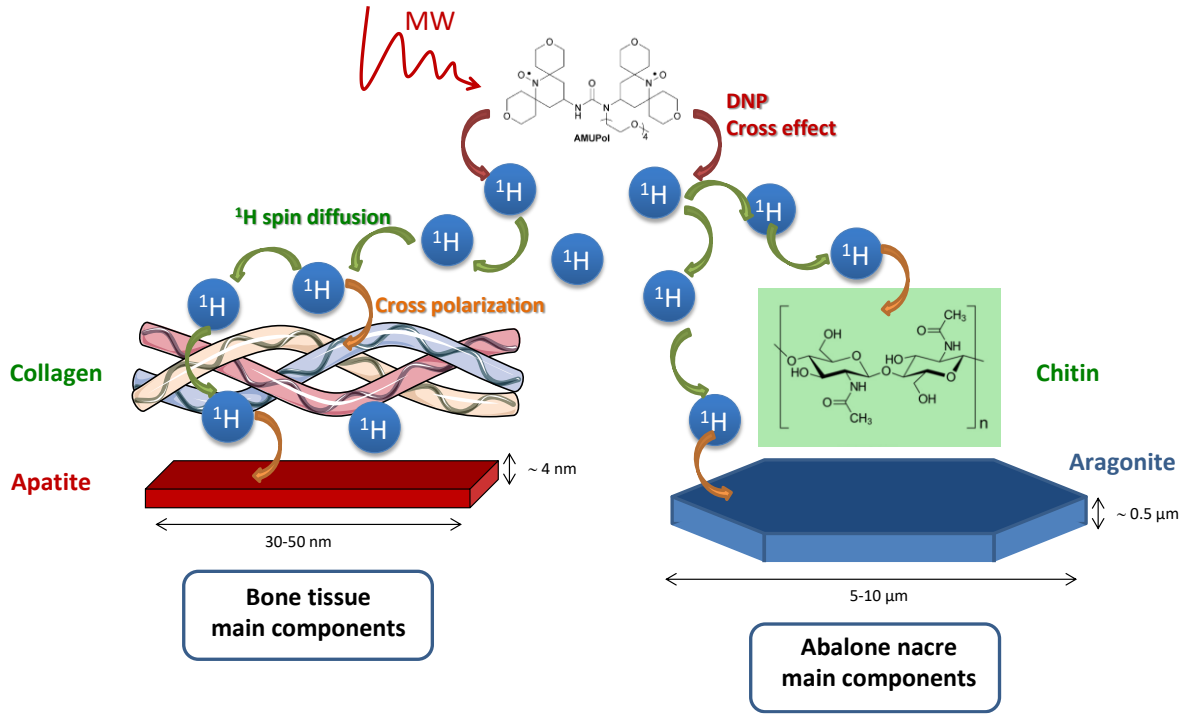

Figure 1. Schematic representation of the DNP SENS approach for the study of cortical bone and nacreous shell.

Materials and Method

Biological samples

The cortical bone tissue sample originates from a two-year-old healthy French sheep. This sample has been extracted from the distal femoral metaphysis, and conserved 24 hours under sterile conditions before analysis. The study was reviewed and approved by the IMM Recherche's Institutional Animal Care and Use committee (IACUC) prior to starting. The animal research center (IMMRecherche) received an approval (n°75-14-01) on September 08th, 2008 by the "Sous-Direction de la protection Sanitaire" of the French Authorities.

One year-old European abalone, *Haliotis tuberculata,* specimens were obtained from *France Haliotis* farm (Plouguerneau, France). After dissection, shells measuring around 1 cm long were washed with distilled water before analysis.

^{13}C and ^{31}P DNP SENS CPMAS spectroscopy

DNP SENS experiments were performed on a Bruker spectrometer 400 MHz magnet equipped with an Avance III HD console and a 3.2 mm LT-MAS probe in the ^{1}H-^{31}P-^{13}C configuration performed at approximately 105 K. DNP was achieved by continuously irradiating the sample with microwaves (MW) at 263 GHz generated by a Bruker gyrotron (9.4 T) and delivered to the probe by a waveguide. The microwave power was optimized so as to obtain maximum enhancement. The cross effect matching condition was set to the maximum positive enhancement of AMUPol using the sweep coil of the spectrometer magnet. Sapphire rotors were used for optimal microwave penetration.

Intact biological samples were first crushed into a mortar until the particles size looked uniform. However, the particle size is inhomogeneous and is ranging from 5 to 100 µm (**Fig. S1**). Powders are then impregnated by 12 mM AMUPol solution in D_2O/H_2O (vol. ratio: 90/10) or Glycerol/D_2O/H_2O (vol. ratio: 60/30/10). The biological samples were equilibrated both at ambient temperature and ambient pressure during 12 and 24 h for cortical bone and nacreous shell, respectively. The sample was transferred in a 3.2 mm sapphire rotor, sealed with polytetrafluoroethylene insert to prevent loss of solvent during the measurements and closed with a zirconia cap. The typical mass of the analyzed samples is about 20 mg. The rotor was inserted in the cold DNP probe to perform the DNP SENS experiments.

Carbon-13 and phosphorus-31 DNP enhancement factors (ε_{CP}) were determined by scaling the intensities of the cross-polarization (CP) spectra with or without microwave (MW) irradiation. DNP SENS CPMAS spectra were recorded with a ^{1}H spin-lock radio-frequency (RF) field set at 100 kHz (at the maximum of the ramp) and a ^{13}C / ^{31}P spin lock RF field of 43.1 and 68.5 kHz respectively. A 70% to 100% ramp was used for the spin-lock pulse on ^{1}H. SPINAL-64 decoupling[23] was applied at a 100 kHz nutation frequency on ^{1}H during the acquisition period. DNP SENS two-dimensional (2D) HETCOR spectra were acquired with eDUMBO-1_{22} homonuclear decoupling during the ^{1}H t_1 evolution period to enhance resolution in the proton dimension.[24] SPINAL-64 decoupling was applied at a RF field strength of 100 kHz during the t_2 evolution period. Quadrature detection was achieved using States-TPPI by incrementing the phase of the proton spin-lock pulse of the CP step.[25] The MAS rate was set at 12.5 kHz for all experiments.

One-dimensional {^{1}H}^{13}C{^{31}P} DNP CP REDOR[26] experiments were acquired using a 180° pulse length of 7.3 µs on ^{31}P to reintroduce the heteronuclear ^{13}C-^{31}P dipolar couplings. A total of 176 scans were accumulated for each 1D experiment.

For an heteronuclear spin pair the REDOR dephasing has the form:

$$1 - \frac{S(t)}{S_0} = \frac{1}{4\pi} \int_{\alpha} \int_{\beta} \left[1 - \cos(2\sqrt{2} D t \sin 2\beta \sin \alpha)\right] \sin\beta \, d\alpha \, d\beta \quad ,$$

where α and β are the Euler angles representing the internuclear vector orientation in the laboratory frame, in a powder these angles are summed over all possible orientations. D ($D = \frac{\mu_0 \gamma_I \gamma_S}{4\pi r^3}$) is the dipolar coupling. The simulations of the REDOR dephasing curves were done using a homemade program. In the calculations we have summed the relative contributions of two ^{13}C populations: *i*) a ^{31}P-^{13}C spin pair contribution of fixed dipolar coupling (*i.e*. of fixed distance). This population corresponds to carbons standing at short distances of phosphorous atoms and governs the dephasing rate. *ii*) Uncoupled ^{13}C nuclei corresponding to carbons that are far from phosphorous and that give no dephasing contribution to the REDOR curve. This population affects the value of the plateau of the dephasing curve.
The data were fitted by varying the dipolar coupling and the fraction of uncoupled nuclei.

Scanning Electron Microscopy

Scanning Electron Microscopy (SEM) was carried out on an ULTRA Plus microscope (Zeiss, Oberkochen, Germany) operating at 5 kV acceleration voltage. The crushed bone tissue sample was deposited on an aluminum stud using conductive carbon adhesive stickers, and was subsequently coated with approximately 5 nm of Au/Pd prior to imaging.

Results and discussion

1. Cortical bone

1.1. Bone apatite surface

Bone tissue is a natural hybrid composite material resulting from an intimate association of a mineral phase with an organic matrix, mainly composed of type I collagen.[27] Type I collagen is a structural protein found in the extracellular space of various connective tissues. The amino-acids form triple-helices assembled into elongated fibrils.[28] The mineral phase corresponds to nanosized carbonated apatite crystals of platelet morphology (~1–5 nm in thickness, ~10–40 nm in width and ~20–100 nm in length.)[29] whose c-axis is aligned along the long axis of the collagen fibrils.[2] Recent data propose that bone mineral platelets are formed by the lateral association of needle-like nanocrystals.[30] Bone apatite is known to possess compositional and structural similarities with synthetic stoichiometric hydroxyapatite (Hap), $Ca_{10}(PO_4)_6(OH)_2$. However, in contrast to stoichiometric Hap, bone apatite is structurally disordered, and compositionally nonstoichiometric due to the incorporation of a substantial amount of anionic (CO_3^{2-}) and cationic (Na^+, Mg^{2+}) substitutions, as well as to the presence of ion vacancies into the crystalline structure.[31] The most relevant of these substitutions in biological apatites are the replacement of the PO_4^{3-} (B-type substitution) and/or OH^- anions (A-type substitution) by CO_3^{2-} ions (up to 5–8 weight %). Bone apatite is also characterized by a so-called "hydrated disordered surface layer" of ~0.8 nm thickness that is mainly composed of divalent species such as Ca^{2+}, HPO_4^{2-}, CO_3^{2-} and structural H_2O.[32] Such "hydrated disordered surface layer" was also identified in biomimetic nanocrystalline apatite.[33] Recently, we evidenced that this hydrated disordered layer is analogous to an amorphous calcium phosphate (ACP) phase[34,35] and is involved in the stacking of the apatite platelets along their c-axis through the interaction with water molecules.[8,36]

The mineral component of bone tissue can be revealed by the ^{31}P DNP SENS CPMAS experiments as reported in **Fig. 2a** (t_{CP} = 5 ms). A single resonance characteristic of bone apatite is observed around 3 ppm (with a line width FWHM = 5 ppm) and slightly asymmetric (shoulder on the left side). The DNP enhancement factor $\varepsilon_{CP\ 31P}$ is found to be around 40 (±2) according to different experiments conducted on similar samples. On the other hand, the organic fraction is observed in the ^{13}C DNP SENS CPMAS spectrum (t_{CP} = 2 ms; **Fig. 2b**) that displays the characteristic ^{13}C resonances of type I collagen, in particular of its main amino-acids, glycine (Gly), proline (Pro) and hydroxyproline (Hyp). We also note the strong resonance centered at 174 ppm corresponding to carbonyls belonging to protein backbones and to carboxyl groups of acidic residues. In addition, a shoulder at 170 ppm is observed that is commonly assigned to CO_3^{2-} present as substitution ions in the apatite crystal lattice.[37] Enhancement factors $\varepsilon_{13C\ CP}$ of around 60 (±5) and 50 (±5) were measured for the aliphatic and carbonyl resonances of collagen, respectively; according also to different experiments conducted on similar samples.

First, we note the ability of DNP to significantly enhance the different NMR signals of bone tissue. The overall profiles of the ^{31}P and ^{13}C DNP SENS CPMAS spectra are similar to those obtained by conventional, room temperature NMR experiments reported in literature,[10,38] both in terms of resonance number and relative positions. This indicates that neither the impregnation by the DNP polarizing solution, nor the cryogenic temperature of the sample (100 K) leads to a structural modification of the bone tissue. We also note that the ^{13}C spectrum of **Fig. 2b** exhibits broader

resonances than that reported on a fresh and hydrated bone sample at ambient temperature but is similar to what was observed for dry bone samples.[39] We ascribe this broadening to the low temperature of the sample in DNP conditions that reduces the dynamic of collagen, leading to a distribution of chemical shifts (inhomogeneous broadening). The overall structure of bone tissue is thus preserved and DNP SENS spectra can be safely analyzed leading to confident structural conclusions (see **Fig. S2**).

Second, we note that the $\varepsilon_{CP\ 31P}$ and $\varepsilon_{13C\ CP}$ are rather high (40 and between 50 and 60, respectively), which may be surprising at first sight as the bone sample investigated here corresponds to cortical bone *i.e.* a dense tissue that does not possess any specific surface area. Nevertheless, compact bone is a hydrated tissue in which three different levels of porosity are reported: (*i*) the "vascular porosity" that corresponds to the space created during the excavation of the Havers and Volkmann tunnels to allow vascularization of the tissue. This porosity corresponds to the diameter of these tunnels (about 40 µm), and is the largest in size within the cortical bone. (*ii*) The "lacuno-canalicular porosity" refers to the lacunar spaces within the mineralized bone matrix, where is found the osteocytes; as well as the canalicular endings hollowed out by osteocytes in order to form communicating junctions. This porosity corresponds to the diameter of the canaliculi (approximately 0.2 µm). (*iii*) The "collagen-apatite porosity" is the very narrow space that exists between collagen fibrils and apatite particles; porosity the smallest in size, a few nanometers maximum.[40,41,42] The high enhancement factors observed here suggest that the radicals from the polarizing solution (i.e. AMUPol molecules) are able to deeply penetrate cortical bone, including up to the collagen-apatite porosity when the sample is immersed long enough in the DNP solution. In this study, we estimate the optimal time of equilibration between 6 and 12 hours for cortical bone. Singh et al reported recently lower carbon-13 DNP enhancement factors of 30 (versus 50 to 60 in the present study) on cortical bone.[20] According to similarities with their experimental conditions (magnetic field of 9.4 T and polarizing solution of 12 mM AMUPol in H_2O/D_2O (90/10 v/v)), this difference can be explained by shorter impregnation times (2-3 min) in their case. Note that no ^{31}P DNP enhanced NMR experiments were conducted in their study.

Finally, we note that the enhancement factor is slightly higher for the organics where DNP directly occurs from radicals homogeneously distributed inside the extracellular matrix and in particular within collagen fibrils. For the inorganic part, DNP is relayed through ^{1}H spin diffusion inside the protonated apatite particles as the radicals will stand near the surface.

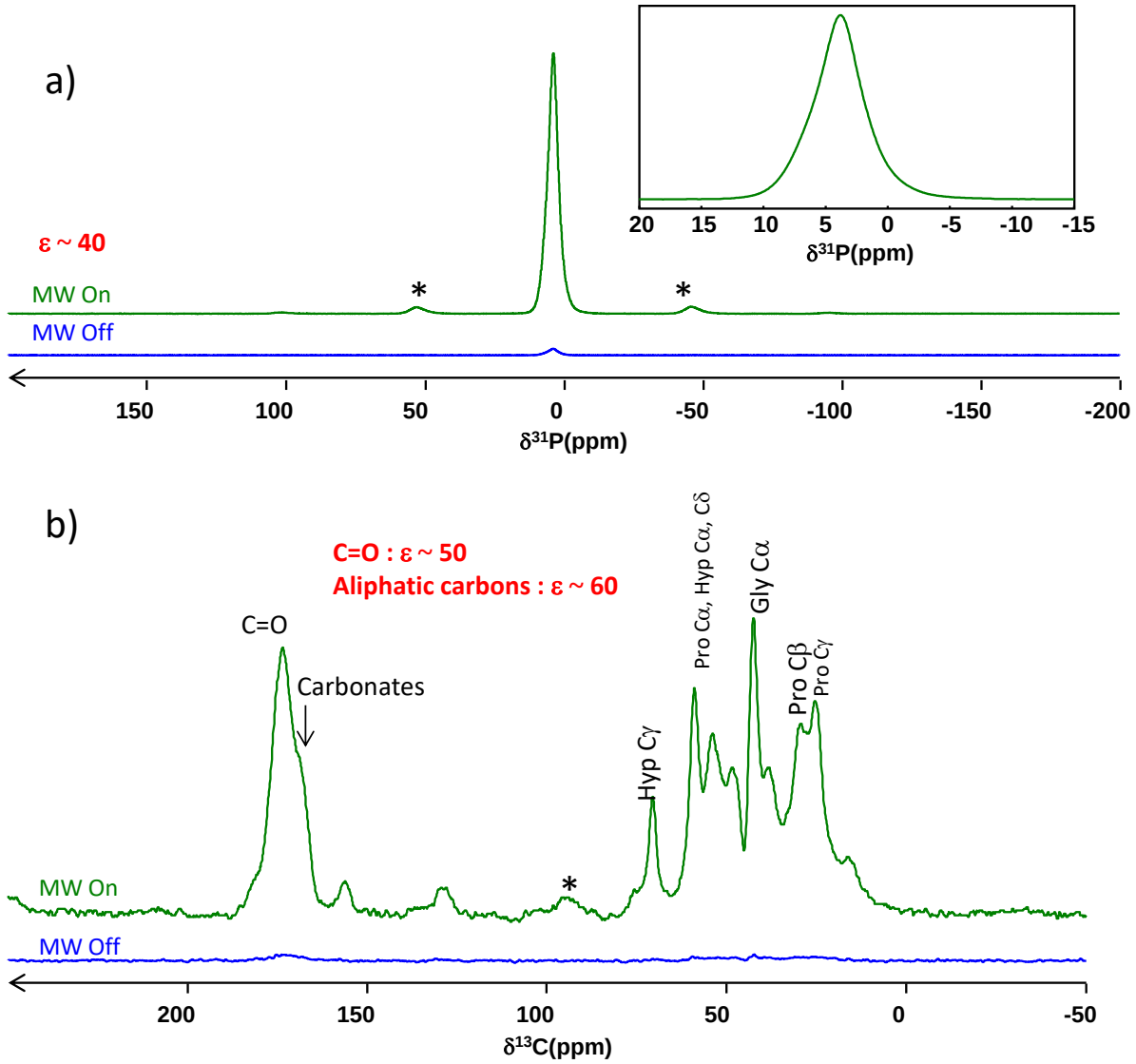

*Figure 2. a) ^{1}H-^{31}P and b) ^{1}H-^{13}C DNP SENS CPMAS spectra of bone (DNP-impregnation solution without glycerol). Main ^{13}C resonances are highlighted. A total of 64 and 128 scans were recorded for ^{13}C and ^{31}P spectra respectively. * denotes spinning side-bands.*

As mentioned above, bone apatite platelets can be described as core-layer particles where an apatitic crystalline core is coated by a hydrated amorphous layer.[8,32,35] The different types of phosphate species composing bone apatite are readily evidenced in the two-dimensional (2D) ^{1}H-^{31}P HETCOR (Heteronuclear Correlation) DNP SENS spectrum (**Fig. 3a**), with a specific emphasis on surface species. Here we note that the drastic sensitivity increase provided by DNP allows one to record such 2D experiments in about 30 minutes.

The hydrogen phosphate ions located in the amorphous-like surface layer of bone apatite appear as a strong broad resonance correlating with water molecules from the DNP polarizing solution (maximum at $\delta(^{1}H)$ = 6.6 ppm) and with protons from $\underline{\mathbf{H}}PO_4^{2-}$ at higher chemical shifts ($\delta(^{1}H)$ up to 15 ppm).[8,34]

The apatitic crystalline core of bone mineral particles containing orthophosphates is also detected as a correlation resonance with OH^- protons from the bulk apatite lattice ($\delta(^1H)$ = 0 ppm). An additional correlation at $\delta(^1H)$ = 1.3 ppm is observed (**Fig. 3b**). We assign this signal to OH^- close to CO_3^{2-} in the apatitic lattice. Such assignment is based on previous studies of ^{13}C-labelled CO_3^{2-}-substituted synthetic apatite where ^1H-^{31}P-^{13}C double CPMAS experiments have highlighted such characteristic resonance that had been assigned to OH^- near CO_3^{2-} in a B-type substitution position.[43] Such resonance is difficult to observe by conventional NMR. According to our knowledge, it was never mentioned and assigned before for bone apatite. Bulk hydroxyl ions in the (radical free) bone mineral particles (thickness ~ 4 nm) here are expected to be polarized by relayed DNP by proton spin diffusion.[22,44,45]

Extracting the ^{31}P slices from the 2D experiment (**Fig. 3c**) allows the comparison of the corresponding phosphates resonances in the three detected environments (amorphous surface, bulk lattice, CO_3^{2-}-containing bulk lattice) and highlights their differences in terms of structural environment: (*i*) HPO_4^{2-} in the amorphous layer displays a broad and slightly asymmetric line shape characteristic of their disordered environment ($\delta(^{31}P)$ = 3 ppm; FWHM = 5.3 ppm); (*ii*) PO_4^{3-} in the apatitic bulk are slightly upfield shifted ($\delta(^{31}P)$ = 2.9 ppm) and exhibit thinner line width (FWHM= 2.7 ppm); (*iii*) finally, PO_4^{3-} close to B-type CO_3^{2-} exhibit a broader line width (LW= 3.3 ppm) due to a local disorder induced by the ionic substitution.

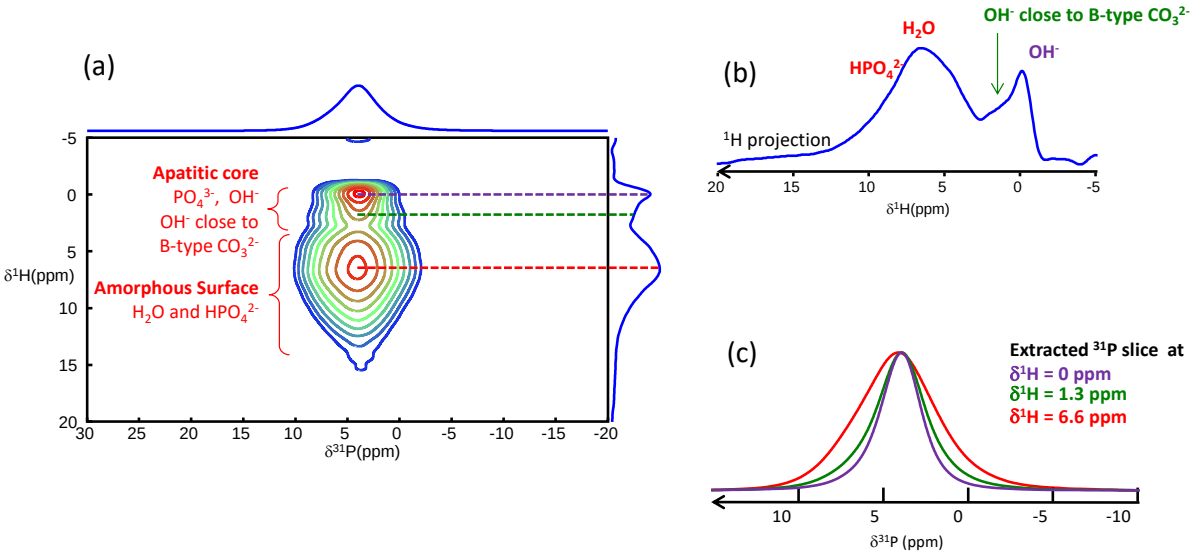

Figure 3. (a) ^1H-^{31}P DNP SENS HETCOR spectrum of bone (t_{CP} = 5 ms; DNP-impregnation solution without glycerol), (b) corresponding ^1H projection, (c) ^{31}P traces extracted at $\delta(^1H)$ = 0, 1.3 and 6.6 ppm. A total of 16 scans were recorded with 128 t_1 increments, an increment step size of 60 µs, a recycle delay of 2 s.

Type I collagen is the most abundant protein in mammals and the major organic constituent of various connective tissues such as tendon, skin, dentin or bone. The most common amino acid motif in collagen respects the following sequence glycine-X-Y where about third of the X and Y

residues are proline and hydroxyproline, respectively. The ^{1}H-^{13}C DNP SENS HETCOR spectrum (t_{CP} = 500 µs) of the bone sample shown in **Fig. 4** displays the characteristic correlation peaks of collagen for the aliphatic ($\delta(^{13}C)$ from 10 to 80 ppm) and C=O resonances ($\delta(^{13}C)$ from 160 to 185 ppm). At this contact time, under DNP conditions, we observe correlations with both NH ($\delta(^{1}H)$ at around 9 ppm) and aliphatic protons ($\delta(^{1}H)$ between 1.7 and 4.3 ppm) for all carbon-13 resonances. In particular we note a strong correlation of Gly Cα carbons with NH groups as expected (dashed line in **Fig. 4**).

The shoulder around 170 ppm that is usually assigned to CO_3^{2-} of bone apatite as B-type substitution is also observed but, surprisingly, there is no correlation with bulk apatitic hydroxyls (expected around $\delta(^{1}H)$ = 0 ppm). Instead, the main correlation peak is centered at $\delta(^{1}H)$ = 3.7 ppm. Therefore, we postulate that this shoulder mainly comes from C=O organic carbons and that the fraction of inorganic carbonates at a similar chemical shift position is too low (between 5 and 8%w/w in bone mineral[3]) to be evidenced through ^{1}H-^{13}C HETCOR spectra.

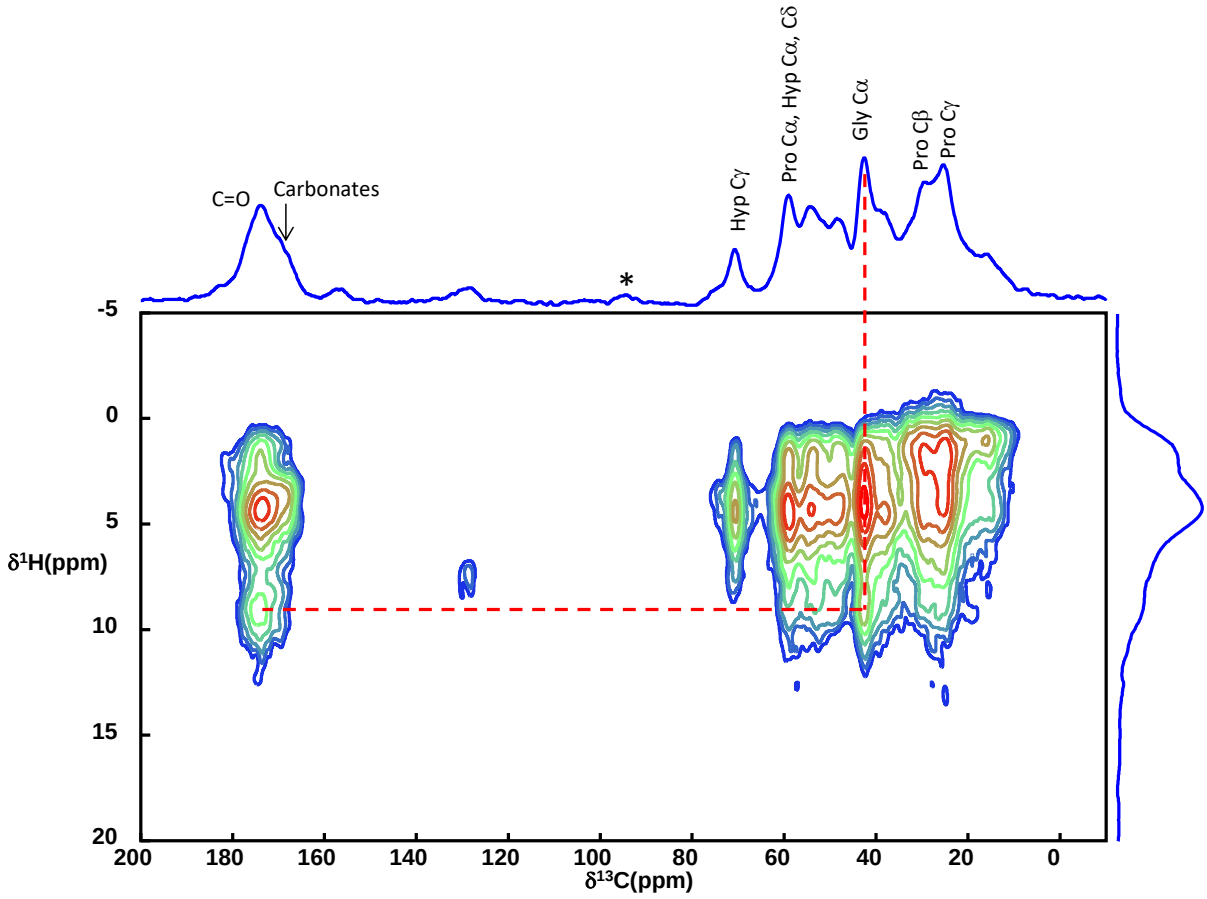

*Figure 4. (a) ^{1}H-^{13}C DNP SENS HETCOR spectrum of bone (t_{CP} = 500 µs; DNP-impregnation solution without glycerol). A total of 32 scans were recorded with 96 t_1 increments, an increment step size of 60 µs, a recycle delay of 2 s. * denotes spinning side-bands.*

1.2. Bone apatite organo-mineral interface

The nature of the organo-mineral interface in bone has been widely debated in the literature as the organic matrix is described to direct the formation of bone mineral. In particular, non-collagenous proteins (NCPs) are proposed to control the nucleation and growth of transient calcium

phosphate phases (such as ACP) and monitor their transformation into bone apatite.[46,47] The collagen matrix itself is also proposed as an essential actor in such process.[48] Solid state NMR studies contributed to the atomic-scale structural investigation of the organo-mineral interface through $^{13}C\{^{31}P\}$ REDOR experiments as the nuclei involved are predominantly located in distinct domains: bone apatite for ^{31}P and the extracellular matrix for ^{13}C. As a result, other species than protein such as glycosaminoglycans[49] and citrate ions[50,51] have been identified to be in close interaction with bone apatite in mature bone tissue. The REDOR has also been used to investigate the role of mineralizing proteins such as osteocalcin and osteopontin at the organic-inorganic interface in bone.[52]

Nevertheless, such $^{13}C\{^{31}P\}$ REDOR experiments are particularly time consuming on natural tissues with conventional MAS NMR spectroscopy. Noticeably, the total experimental time used by Hu et al.[50] to record four REDOR points (*i.e.* four ^{13}C REDOR spectra with ^{31}P irradiation and four ^{13}C REDOR spectra without ^{31}P irradiation) was 19 days! Given the signal enhancement factors discussed previously, the experimental time of similar REDOR experiments should be drastically reduced with DNP.

Figure 5a displays $\{^{1}H\}^{13}C\{^{31}P\}$ DNP CP REDOR spectra of cortical bone (recoupling time $R\tau$ = 14.1 ms). The dephasing of carboxylate (COO^-) and quaternary carbon (Cq) resonances from citrate ions (at 181 and 75.6 ppm, respectively) is observed in agreement with published data.[49,50] We note also the dephasing of CO_3^{2-} from the apatitic lattice of bone mineral.

In order to evaluate the distance between citrate moieties and bone apatite surface, variation of $R\tau$ was undertaken. The REDOR curves corresponding to COO^- and Cq resonances are plotted in **Figure 5b-c**. A total of 24 points ($R\tau$ up to 24.1 ms *i.e.* 185 rotor periods) were recorded in 11 hours. Numerical analysis allows P-C distance determination together with the fraction of citrate involved in the apatite binding. According to best fits, COO^- and Cq groups are located at 0.5 nm from the apatite surface. Such distances are in good agreement with published data, even if they are found a little bit longer than in previous measurements (3.5 and 4.5 Å for COO^- and Cq, respectively).[50] This difference is somehow difficult to interpret but we should note a difference in sample preparation with the study of Hu *et al.*[50] Freshly extracted bone sample was used in the present study whereas Hu *et al.*[50] studied a cryomilled and organic solvent (methanol/chloroform) treated sample (femur cortical bone from a four-year-old cow). Such procedure might destabilize the ultrastructure and/or dehydrate bone tissue. The removal of water molecules tightly bonded to the surface of bone mineral surface induces the collapse of the collagen network and might lead to a stronger adsorption of citrate ions onto the surface.

Thanks to the signal enhancement provided by DNP, REDOR experiments could be recorded up to 24.1 ms recoupling time allowing the observation of a plateau of the dephasing signal that is related to the fraction of citrate ions involved in the interaction with bone apatite. Assuming that the resonances observed at 181 and 75.6 ppm are only related to citrate, we note that 80% of Cq exhibit a significant dephasing meaning that 80% of citrate ions present in the bone tissue are involved with bone surface binding. Similarly, only 50% of COO^- are concerned by a significant dephasing. Following this observation, we can conclude that for one bonded-citrate only two out of three carboxylate functions ($0.5/0.8 = 0.625 \approx 0.67$) are bonded to the mineral surface. Such result is agreement with the bone mineral model developed by Davies *et al.*[51] in which citrate ions are entrapped within an OCP-like structure as a structurally organized layer. Through numerical calculation they propose that

one carboxylic group from citrate "is not coordinated to any calcium anions and is dangling into the water channel" in coherence with our experimental data.

No strong dephasing was observed for type I collagen resonances evidencing "long" distances between collagen fibrils and bone mineral platelets. The absence of direct bonding in mature bone was already proposed[53] and is coherent with the presence of confined water molecules in-between apatite particles and collagen fibrils, namely the interstitial water present in the collagen-apatite porosity.[54]

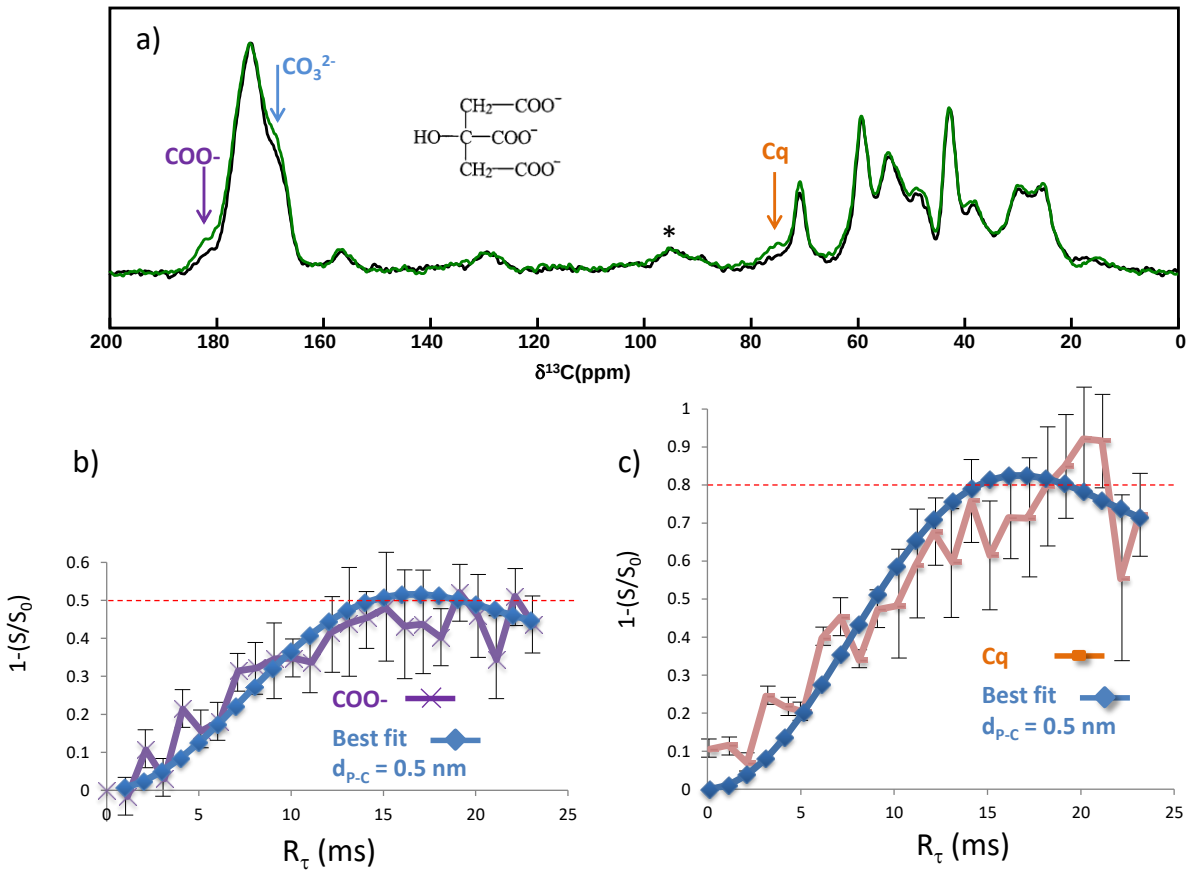

*Figure 5 : a) {^{1}H}^{13}C{^{31}P} DNP CP REDOR spectra of cortical bone recorded with (black) and without ^{31}P (green) irradiation (R_τ = 14.1 ms; DNP-impregnation solution without glycerol; * denotes spinning side-bands). Dephasing evolution of b) COO^- (181 ppm) and c) Cq (75.6 ppm) resonances with increasing recoupling time (R_τ). Best fits are in blue, dephasing plateau is indicated as a red dashed line and error bars are in black.*

2. European abalone Haliotis tuberculata *shell*

2.1. Aragonite surface

The shell of European abalone *Haliotis tuberculata* is a composite hybrid material composed of calcium carbonate $CaCO_3$ intimately associated to an organic matrix. In the adult shell, three distinct layers are identified: an outer organic layer (the periostracum), an intermediate spherulitic layer and an innermost nacreous layer.[55] The mineral phase represents about 95 w% of the material whereas the remaining 5 w% constitutes the organic matrix. The mineral phase in European abalone is found as micrometric aragonite crystals for which the morphology differs as a function of their location into the shell: irregular spherulitic crystals in the spherulitic layer and pseudo-hexagonal tablets in the nacre layer. Whatever the layer, the aragonite crystals are embedded in an organic matrix mainly composed of polysaccharide namely β-chitin. In this mineralized tissue both the organic (β-chitin) and the inorganic ($CaCO_3$) counterparts are composed of carbons atoms. Moreover, European abalone shell is a dense 3D organized tissue which is not vascularized and does not possess any particular identified porosity. Thus, analyzing mineral surfaces and interfaces in European abalone shell is much more challenging than in bone.

Aragonite crystals from mollusks shell have also a protonated disordered layer of ~5 nm thickness that was identified as amorphous calcium carbonate (ACC) in mature nacre in *Haliotis laevigata* [7,56] or in forming nacre tablets in *Perna Viridis*.[57] Recently, different disordered carbonate environments were identified in *Perna canaliculus* and assigned to "exposed carbonate", at the surface of the aragonite crystals in interaction with the organics molecules, and "buried carbonate" defects within the mineral bulk.[58] Such "buried carbonate" could be associated to intracrystalline organic molecules are entrapped within individual crystallites inducing anisotropic lattice distortions in *Perna canaliculus*.[59]

Here ^{13}C DNP SENS experiments were used to selectively detect exposed carbonates. The ^{13}C DNP SENS CPMAS spectra of *Haliotis tuberculta* shell are displayed in **Fig. 6**. Different resonances can be highlighted as a function of the CP contact time. At short CP contact time we observe mainly the resonances of the organic moieties (**Fig 6a**), with an enhancement factor $\varepsilon_{13C\ CP}$ of around 100. The resonances of β-chitin are identified (**Fig. S3**), in particular the C3/C5 resonance at 73 ppm, confirming the presence of this polysaccharide in the interlamellar matrix of abalone nacre.[60] Interestingly, additional resonances are observed in the range 20 to 50 ppm corresponding to proteinaceous material.[61] The contribution of the organic carbons is strongly attenuated at longer CP contact times, while the resonances of carbonates in the protonated environments of aragonite become clearly visible, among which a narrow resonance at 170.5 ppm (**Fig 6b**). This spectral edition is permitted by differential longitudinal relaxation times along the applied radio-frequency pulse ($T_1\rho(^1H)$), that are much longer for resonances of the inorganic part.[56,58] An enhancement $\varepsilon_{13C\ CP}$ of 11 was measured on the carbonate resonance with a glycerol-containing polarizing solution (versus $\varepsilon_{13C\ CP}$ of 6 without glycerol; **Fig. S4**). **Fig 6c** shows an expansion of the CP MAS spectra in the low field area and a comparison with a ^{13}C single pulse spectrum. On the latter a single thin resonance at $\delta(^{13}C)$ = 171.5 ppm is observed that corresponds to carbonate from crystalline aragonite.[11] The resonances of the organic matrix and of β-chitin in particular are not observed due to their very low

proportion in the sample (less than 5 w%). Exposed carbonates, observed in the CPMAS spectrum at long contact time, exhibit a slightly shifted resonance at higher field (170.5 ppm) and of larger linewidth due to higher local disorder as compared to carbonates in crystalline environment. At short contact time, the spectrum is dominated by the resonances of the organic matrix. This detailed analysis is made possible by the extremely high sensitivity of DNP SENS and illustrates the great potential of this approach to specifically enlighten surface species in biological calcium carbonates.

As expected and as is the case for the bone tissue, $\varepsilon_{13C\ CP}$ is higher for the organic matrix, where DNP occurs directly, than for the inorganic part, where DNP is relayed through ^{1}H spin diffusion inside the amorphous layer. Overall, these results indicate as was the case for the bone apatite, that the radical solution is able to penetrate the organic matrix when the equilibration time is long enough (24 h here) and polarize efficiently both the organic and inorganic domains.

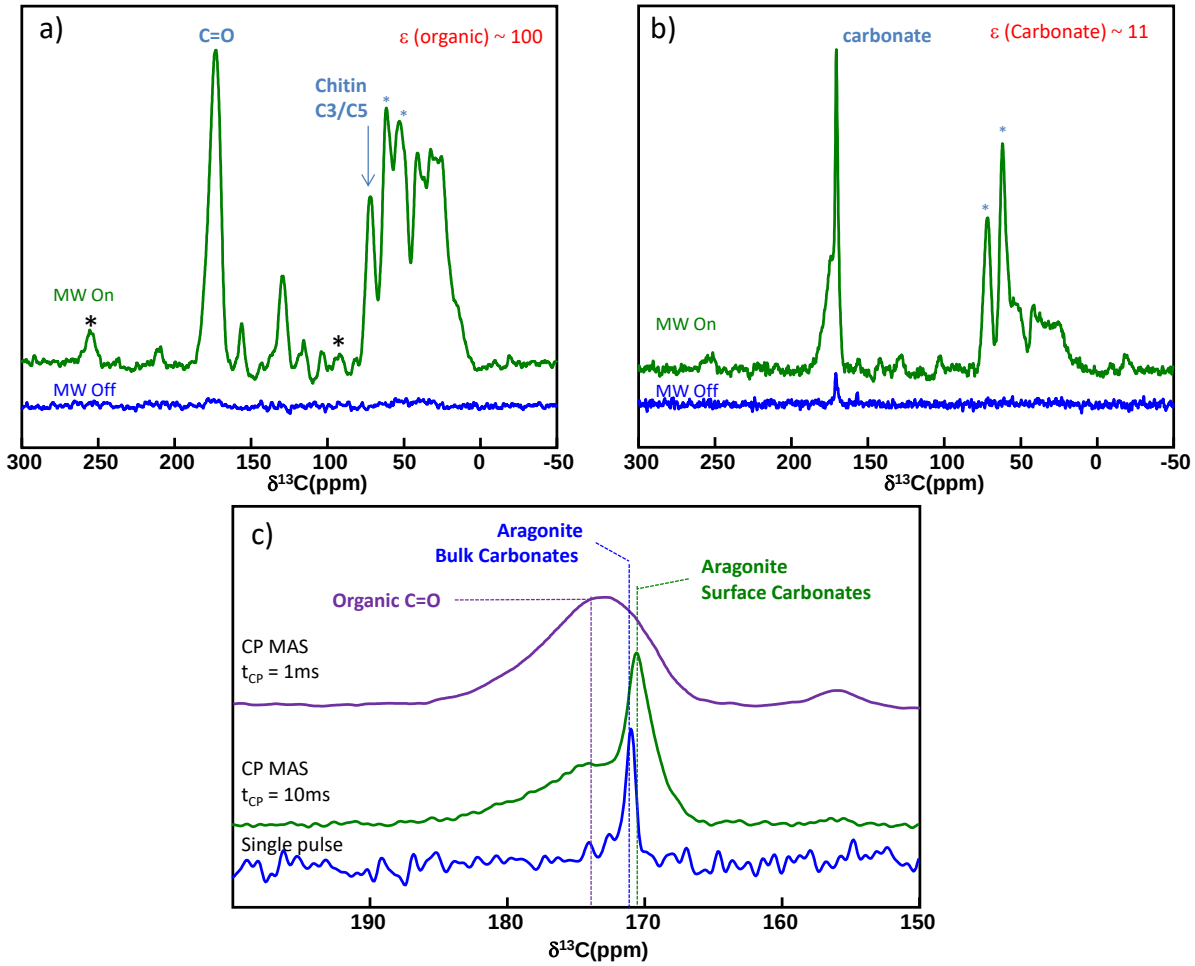

Figure 6 :^{1}H-^{13}C DNP SENS CPMAS spectra (DNP-impregnation solution with glycerol) of European abalone shell : a) t_{CP} = 1 ms; b) t_{CP} = 10 ms. The number of scans was 1200 and 128 in a) and b) respectively. c) Comparison of the ^{1}H-^{13}C DNP SENS CPMAS spectra and the ^{13}C direct acquisition NMR spectrum (4 scans with a recycle delay of 600 s). Blue stars denote ^{13}C resonances from glycerol. Black stars denote spinning side-bands.

2.2. Organo-mineral interface

Two-dimensional ^{1}H-^{13}C DNP SENS HETCOR spectra of nacreous shell could also be recorded in extremely short experimental times (16 min here). The HETCOR spectrum corresponding to a contact time of t_{CP} = 10 ms is depicted in **Fig. 7** and reveals the nature of the exposed carbonates. A strong correlation peak at $\delta(^{1}H)$ = 14 ppm characteristic of HCO_3^- ion[62] demonstrates that a large amount of exposed carbonates in the European abalone shell appears as protonated in the form of bicarbonates ions. This result is coherent with similar analyses of nacre from *Haliotis laevigata*[7] and of shell from *Perna canaliculus*.[58] Moreover, we do not observe any signal related to water molecules, indicated that such surface species are not strongly H_2O-bonded unlike bone mineral. Taking into account that biomimetic amorphous calcium carbonate (ACC) do not contain any substantial amount of bicarbonate ions,[62,63] [64] it seems unrealistic to assign the disorder layer around aragonite crystal in nacreous shells to ACC *stricto sensu* but rather to a bicarbonate-containing disordered phase.

The analysis of the 2D ^{1}H-^{13}C DNP SENS HETCOR spectrum also provides insight into the nature of the organo-mineral interface. A strong correlation at $\delta(^{1}H)$ = 2.6 ppm is observed for exposed bicarbonates indicating a close proximity with aliphatic moieties. While such resonance is difficult to interpret due to a lack of resolution, it remains a direct signature of the organo-mineral interface. According to Kono et al.,[65] this cross-peak could be related to the H3 protons of β-chitin (2.8 ppm) but we also might consider that this signal is related to the presence of acidic proteins that are known to control the nucleation and growth of the mineral phase in such nacreous shell.[66] Nevertheless, this example is a nice illustration of the potential of DNP MAS approaches for the investigation of organo-mineral interfaces in carbonate-based calcified tissues.

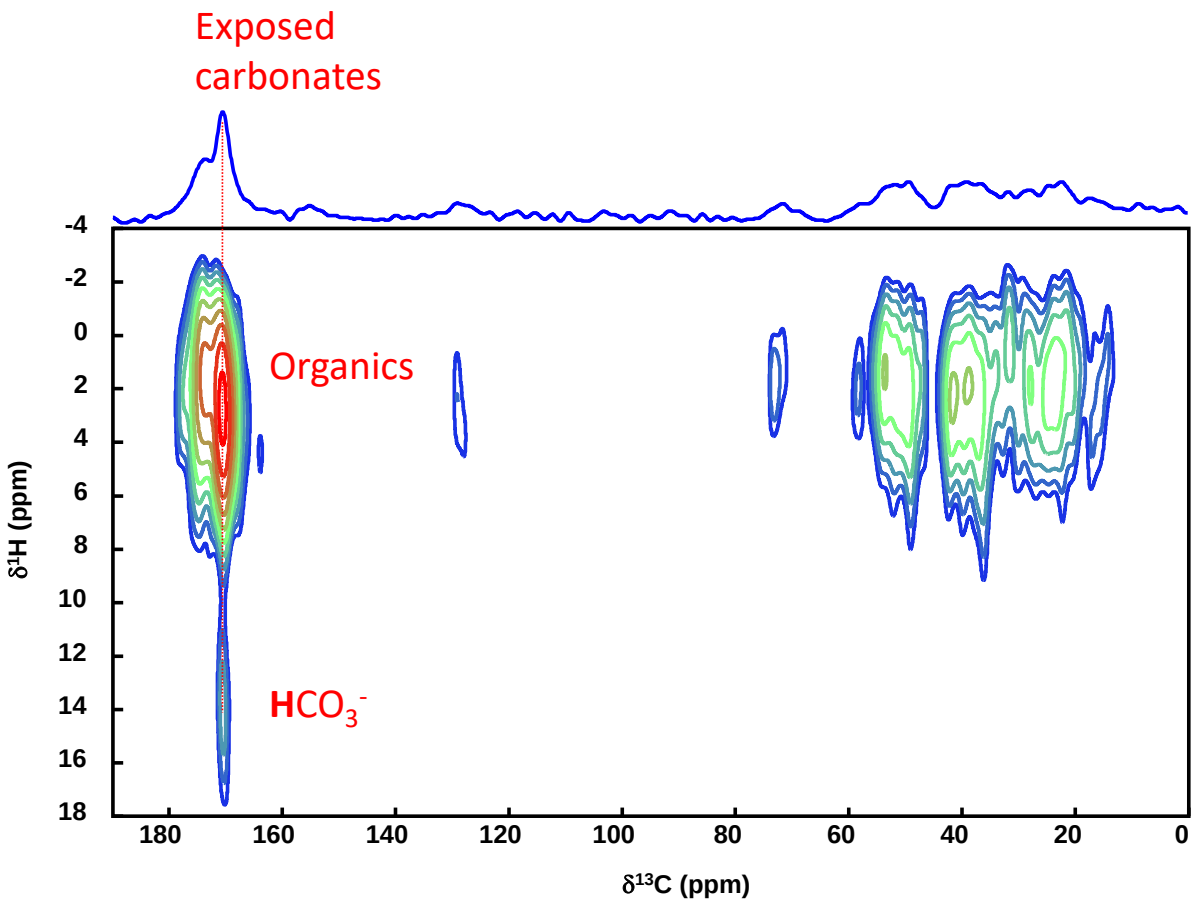

Figure 7 : ^{1}H-^{13}C DNP SENS HETCOR spectrum of European abalone shell (t_{CP} = 10 ms; DNP-impregnation solution without glycerol). A total of 24 scans were accumulated with 20 t_1 increments, an increment step size of 60 µs, and a recycle delay of 2 s.

Conclusion

In this communication we demonstrated that DNP SENS is a method of choice to study biological mineralized tissues in general, and surfaces / interfaces of their corresponding biominerals in particular. Even if bone and nacreous shell do not possess any identified mesoporosity, the impregnation of the materials by aqueous-based radical solutions was found to efficiently distribute the radicals probably due to the high intrinsic hydration level of these biomineralized tissues. Concerning the inorganic fraction, signal enhancement factors 40 and 11 for bone apatite and nacreous aragonite were reported, respectively. We demonstrated that the surface structure of the crystals could be readily probed through ^{1}H-^{31}P or ^{1}H-^{13}C DNP SENS HETCOR experiments evidencing the presence of hydrogenphosphates (bone mineral) and bicarbonates (aragonite) as exposed species.

Higher signal enhancement factors were found for the organic matrix, both for cortical bone (between 50 and 60) and for nacreous shell (up to 100). This result is particularly promising in the case of nacreous shell as the nature of the biomacromolecules composing mollusk shell layers (periostracum, spherulitic/prismatic or nacreous layer) is still under debate.[61] In that context, we demonstrated that ^{13}C DNP NMR experiments could reveal the presence of chitin as well as proteinaceous material in European abalone *Haliotis tuberculata* shell.

Finally, we demonstrated that organo-mineral interactions could be probed at the atomic level with high sensitivity. In particular, reliable $^{13}C\{^{31}P\}$ REDOR experiments were performed in a few hours, leading to the determination of distances and molar proportion of citrate bonded to bone mineral in native compact bone. Our data suggests that a significant proportion of citrate (20 %) from cortical bone tissue is not bonded to apatite crystals and that the adsorption mode of citrate ions involves two out of three carboxylate groups.

Acknowledgments

This work was supported by French state funds managed by the ANR within the Investissements d'Avenir programme under reference ANR-11-IDEX-0004-02, and more specifically within the framework of the Cluster of Excellence MATISSE led by Sorbonne Universités. This work was also supported by the Région Bretagne. Financial support is acknowledged from the ERC Advanced Grant No.320860. European abalone *Haliotis tuberculata* samples were kindly provided by France Haliotis (Kerazan, Plouguernau, France).

[1] H. A. Lowenstam, S. Weiner, On biomineralization, Oxford University Press (1989)
[2] M. J. Glimcher, Bone: nature of the calcium phosphate crystals and cellular, structural, and physical chemical mechanisms in their formation, Rev. Mineral. Geochem. 64 (2006) 223–282.
[3] C. Rey, C. Combes, C. Drouet, M. J. Glimcher, Bone mineral: update on chemical composition and structure, Osteoporos. Int. 20 (2009) 1013–1021.
[4] S. Weiner, P. M. Dove, An overview of biomineralization processes and the problem of the vital effect, Rev. Mineral. Geochem. 54 (1) (2003) 1–29.
[5] Y. Wu, J. L. Ackerman, H.-M. Kim, C. Rey, A. Barroug, M. J. Glimcher, Nuclear magnetic resonance spin-spin relaxation of the crystals of bone, dental enamel, and synthetic hydroxyapatites, J. Bone Miner. Res. Off. J. Am. Soc. Bone Miner. Res. 17 (2002) 472–480.
[6] S.-J. Huang, Y.-L. Tsai, Y.-L. Lee, C.-P. Lin, J. C. C. Chan, Structural model of rat dentin revisited, Chem. Mater. 21 (2009) 2583–2585.
[7] N. Nassif, N. Pinna, N. Gehrke, M. Antonietti, C. Jäger, H. Cölfen, Amorphous layer around aragonite platelets in nacre, Proc. Natl. Acad. Sci. U. S. A. 102 (2005) 12653–12655.
[8] Y. Wang, S. Von Euw, F.M. Fernandes, S. Cassaignon, M. Selmane, G. Laurent, G. Pehau-Arnaudet, C. Coelho, L. Bonhomme-Coury, M.-M. Giraud-Guille, F. Babonneau, T. Azaïs, N. Nassif, Water-mediated structuring of bone apatite, Nat Mater. 12 (2013) 1144–1153.
[9] M. J. Duer, The contribution of solid-state NMR spectroscopy to understanding biomineralization: atomic and molecular structure of bone, J. Magn. Reson. 253 (2015) 98–110.
[10] K. H. Mroue, A. Viswan, N. Sinha, A. Ramamoorthy, Chapter Six - Solid-state NMR spectroscopy: the magic wand to view bone at nanoscopic resolution, Editor(s): Graham A. Webb, Annual Reports on NMR Spectroscopy, Academic Press, 92 (2017) 365-413.
[11] I. Ben Shir, S. Kababya, A. Schmidt, Molecular-level structure-property relationships in biogenic calcium carbonates: the unique insights of solid-state NMR spectroscopy, Isr. J. Chem. 54 (2014) 74 – 85.
[12] A. J. Rossini, A. Zagdoun, M. Lelli, A. Lesage, C. Copéret, L. Emsley, Dynamic nuclear polarization surface enhanced NMR spectroscopy, Acc. Chem. Res. 46 (2013) 1942–1951.
[13] A. Lesage, M. Lelli, D. Gajan, M. A. Caporini, V. Vitzthum, P. Mieville, J. Alauzun, A. Roussey, C. Thieuleux, A. Mehdi, G. Bodenhausen, C. Coperet, L. Emsley, Surface enhanced NMR spectroscopy by dynamic nuclear polarization. J. Am. Chem. Soc. 132 (44) (2010) 15459–15461.
[14] M. Lelli, D. Gajan, A. Lesage, M. A. Caporini, V. Vitzthum, P. Miéville, F. Héroguel, F. Rascón, A. Roussey, C. Thieuleux, M. Boualleg, L. Veyre, G. Bodenhausen, C. Coperet, L. Emsley, Fast characterization of functionalized silica materials by silicon-29 surface-enhanced NMR spectroscopy using dynamic nuclear polarization, J. Am. Chem. Soc. 133 (7) (2011) 2104–2107.
[15] C. Sauvée, M. Rosay, G. Casano, F. Aussenac, R. T. Weber, O. Ouari, P. Tordo, Highly efficient, water-soluble polarizing agents for dynamic nuclear polarization at high frequency, Angew. Chem. 125 (2013) 11058-11061.
[16] A. Zagdoun, G. Casano, O. Ouari, M. Schwarzwälder, A. J. Rossini, F. Aussenac, M. Yulikov, G. Jeschke, C. Copéret, A. Lesage, P. Tordo, L. Emsley, Large molecular weight nitroxide biradicals providing efficient dynamic nuclear polarization at temperatures up to 200 K, J. Am. Chem. Soc. 135 (34) (2013) 12790–12797.
[17] G. Casano, H. Karoui, O. Ouari, Polarizing agents: evolution and outlook in free radical development for DNP, eMagRes 7 (2018) 195–208.
[18] F. Mentink-Vigier, I. Marin-Montesinos, A. P. Jagtap, T. Halbritter, J. van Tol, S. Hediger, D. Lee, S. T. Sigurdsson, G. De Paëpe, Computationally assisted design of polarizing agents for dynamic nuclear polarization enhanced NMR: the AsymPol family, J. Am. Chem. Soc. 140 (2018) 11013−11019.
[19] P. Berruyer, L. Emsley, A. Lesage, DNP in materials science: touching the surface, eMagRes 7 (2018**)** 93–104
[20] C. Singh, R. K. Rai, F. Aussenac, N. Sinha, Direct evidence of imino acid–aromatic interactions in native collagen protein by DNP-enhanced solid-state NMR spectroscopy, J. Phys. Chem. Lett., 5 (22) (2014) 4044-4048.
[21] D. Lee, C. Leroy, C. Crevant, L. Bonhomme-Coury, F. Babonneau, D. Laurencin, C. Bonhomme, G. De Paëpe, Interfacial Ca^{2+} environments in nanocrystalline apatites revealed by dynamic nuclear polarization enhanced ^{43}Ca NMR spectroscopy, Nat. Commun. 8 (2017) 14104.
[22] C. Leroy, F. Aussenac, L. Bonhomme-Coury, A.Osaka, S. Hayakawa, F. Babonneau, C. Coelho-Diogo, C. Bonhomme, Hydroxyapatites: key structural questions and answers from dynamic nuclear polarization, Anal. Chem. 89 (19) (2017) 10201–10207.
[23] B. M. Fung, A. K. Khitrin, K. Ermolaev, An improved broadband decoupling sequence for liquid crystals and solids, J. Magn. Reson. 142 (2000) 97-101.

[24] B. Elena, G. de Paëpe, L. Emsley, Direct spectral optimisation of proton–proton homonuclear dipolar decoupling in solid-state NMR, Chem. Phys. Lett. 398 (2004) 532-538.
[25] D. Marion, M. Ikura, R. Tschudin, A. Bax, Rapid recording of 2D NMR spectra without phase cycling. application to the study of hydrogen exchange in proteins, J. Magn. Reson. 85 (1989) 393-399
[26] T. Gullion, J. J. Schaefer, Rotational-echo double-resonance NMR, Magn. Reson. 81 (1989) 196−200.
[27] K. Grandfield, V. Vuong & H. P. Schwarcz, Ultrastructure of Bone: hierarchical features from nanometer to micrometer scale revealed in focused ion beam sections in the TEM, Calcif. Tissue Int. 103 (2018), 606–616.
[28] A. Gautieri, S. Vesentini, A. Redaelli, M. J. Buehler, Hierarchical structure and nanomechanics of collagen microfibrils from the atomistic scale up, Nano letters, 11(2) (2011), 757-766.
[29] S. J. Eppell, W. Tong, J. L. Katz, L. Kuhn, M. J. Glimcher, Shape and size of isolated bone mineralites measured using atomic force microscopy, J. Orthop. Res., 19 (2001), 1027–1034.
[30] N. Reznikov, M. Bilton, L. Lari, M. M. Stevens, R. Kröger, Fractal-like hierarchical organization of bone begins at the nanoscale, Science, 360 (2018), eaao2189.
[31] B. Wopenka, J. Pasteris, A mineralogical perspective on the apatite in bone, Materials Science and Engineering: C ,25 (2005), 131-143.
[32] M. Duer, A. Veis, Bone mineralization: Water brings order, Nat. Mater. 12 (2013) 1081–1082.
[33] C. Rey, C. Combes, C. Drouet, H. Sfihi, A. Barroug, Physico-chemical properties of nanocrystalline apatites: implications for biominerals and biomaterials, Mater. Sci. Eng. C 27 (2007) 198-205.
[34] Y. Wang, S. Von Euw, G. Laurent, C. Crevant, L. Bonhomme-Coury, M-M. Giraud-Guille, F. Babonneau, N. Nassif, T. Azaïs, Impact of collagen confinement vs. ionic substitutions on the local disorder in bone and biomimetic apatites, Mater. Horiz. 1 (2) (2014) 224–231.
[35] S. Von Euw, W. Ajili, T-H-C. Chan-Chang, A. Delices, G. Laurent, F. Babonneau, N. Nassif, T. Azaïs, Amorphous surface layer versus transient amorphous precursor phase in bone – a case study investigated by solid-state NMR spectroscopy, Acta Biomaterialia 59 (2017) 351–360.
[36] S. Von Euw, T-H-C. Chan-Chang, C. Paquis, B. Haye, G. Pehau-Arnaudet, F. Babonneau, T. Azaïs, N. Nassif, Organization of bone mineral: the role of mineral–water interactions, Geosciences 8 (12) (2018) 466.
[37] K. Beshah, C. Rey, M. J. Glimcher, M. Schimizu, R. G. Griffin, Solid state carbon-13 and proton NMR studies of carbonate-containing calcium phosphates and enamel, J. Solid State Chem. 84 (1990) 71–81.
[38] W. Kolodziejski, Solid-state NMR studies of bone, Top. Curr. Chem. 246 (2004) 235–270.
[39] P. Zhu, J. Xu, N. Sahar, M. D. Morris, D. H. Kohn, A. Ramamoorthy, Time-resolved dehydration-induced structural changes in an intact bovine cortical bone revealed by solid-state NMR spectroscopy. J. Am. Chem. Soc. 131 (2009) 17064-17065.
[40] S. C. Cowin, Bone poroelasticity, J. Biomech. 32 (3) (1999) 217–238.
[41] P. Fantazzini, R. Viola, S. M. Alnaimi, J. H. Strange, Combined MR-relaxation and MR-cryoporometry in the study of bone microstructure, Magn. Reson. Imaging 19 (3) (2001) 481–484.
[42] J. Samuel, D. Sinha, J. C.-G. Zhao, X. Wang, Water residing in small ultrastructural spaces plays a critical role in the mechanical behavior of bone, Bone 59 (2014) 199‑206.
[43] F. Babonneau, C. Bonhomme, S. Hayakawa, A. Osaka, Mater. Res. Soc. Symp. Proc. 984 (2007) MM06–05.
[44] A. C. Pinon, J. Schlagnitweit, P. Berruyer, A. J. Rossini, M. Lelli, E. Socie, M. Tang, T. Pham, A. Lesage, S. Schantz, L. Emsley, Measuring nano- to microstructures from relayed dynamic nuclear polarization NMR, J. Phys. Chem. C, 121 (29) (2017) 15993–16005.
[45] A.C. Pinon, U. Skantze, J. Viger-Gravel, S. Schantz, L. Emsley, Core−shell structure of organic crystalline nanoparticles determined by relayed dynamic nuclear polarization NMR, J Phys Chem A, 122 (44) (2018) 8802–8807.
[46] A. George, A. Veis, Phosphorylated proteins and control over apatite nucleation, crystal growth, and inhibition. Chem. Rev. 108 (2008) 4670-4693.
[47] L. C. Palmer, C. J. Newcomb, S. R. Kaltz, E. D. Spoerke, S. I. Stupp, Biomimetic systems for hydroxyapatite mineralization inspired by bone and enamel. Chem. Rev. 108 (2008) 4754-4783.
[48] Y. Wang, T. Azaïs, M. Robin, A. Vallée, C. Catania, P. Legriel, G. Pehau-Arnaudet, F. Babonneau, M-M. Giraud-Guille, N. Nassif, The predominant role of collagen in the nucleation, growth, structure and orientation of bone apatite, Nat. Mater. 11 (2012) 724–733.
[49] E. R. Wise, S. Maltsev, M. E. Davies, M. J. Duer, C. Jaeger, N. Loveridge, R. C. Murray, D. G. Reid, The organic-mineral interface in bone is predominantly polysaccharide, Chem. Mater. 19 (2007) 5055-5057.
[50] Y-Y. Hu, A. Rawal, K. Schmidt-Rohr, Strongly bound citrate stabilizes the apatite nanocrystals in bone. Proc. Natl Acad. Sci. USA 107 (2010) 22425-22429.

[51] E. Davies, K. H. Müller, W. C. Wong, C. J. Pickard, D. G. Reid, J. N. Skepper, M. J. Duer Citrate bridges between mineral platelets in bone, Proc. Natl Acad. Sci. USA,111 (14) (2014) E1354-E1363

[52] O. Nikel, D. Laurencin, S. A. McCallum, C. M. Gundberg, D. Vashishth, NMR investigation of the role of osteocalcin and osteopontin at the organic-inorganic interface in bone, Langmuir 29 (2013) 13873-13882.

[53] R. Kumar Rai and N. Sinha, Dehydration-induced structural changes in the collagenhydroxyapatite interface in bone by high-resolution solid-state NMR spectroscopy, J. Phys. Chem. C, 115 (29) (2011) 14219–14227.

[54] E. E Wilson, A. Awonusi, M. D Morris, D. H Kohn, M. M. J. Tecklenburg, L. W. Beck, Highly ordered interstitial water observed in bone by nuclear magnetic resonance. J. Bone Miner. Res. 20 (2005) 625-634.

[55] S. Auzoux-Bordenave, A. Badou, B. Gaume, S. Berland, M-N. Helléouet, C. Milet, S. Huchette, Ultrastructure, chemistry and mineralogy of the growing shell of the european abalone haliotis tuberculata, J. Struct. Biol., 171 (3) (2010) 277–290.

[56] C. Jäger, H. Cölfen, Fine structure of nacre revealed by solid state ^{13}C and ^{1}H NMR, CrystEngComm, 9 (12), (2007) 1237–1244.

[57] G. Zhang, J. Xu, From colloidal nanoparticles to a single crystal: new insights into the formation of nacre's aragonite tablets, J. Struct. Biol. 182 (1) (2013) 36–43.

[58] I. Ben Shir, S. Kababya, I. Katz, B. Pokroy, A. Schmidt, Exposed and buried biomineral interfaces in the aragonitic shell of perna canaliculus revealed by solid-state NMR, Chem. Mater. 25 (22) (2013) 4595–4602.

[59] B. Pokroy, J. S. Fieramosca, R. B. Von Dreele, A. N. Fitch, E. N. Caspi, E. Zolotoyabko, Atomic structure of biogenic aragonite, Chem. Mater. 19 (13) (2007) 3244–3251.

[60] I. M. Weiss, C. Renner, M. G. Strigl, M. Fritz, A simple and reliable method for the determination and localization of chitin in abalone nacre, Chem. Mater. 14 (2002) 3252-3259.

[61] O. B. A. Agbaje, I; Ben Shir, D. B.Zax, A. Schmidt, D. E. Jacob, Biomacromolecules within bivalve shells: Is chitin abundant? Acta Biomater. 80 (2018) 176-187.

[62] H. Nebel, M. Neumann, C. Mayer, M. Epple, On the structure of amorphous calcium carbonates - A detailed study by solid-state NMR spectroscopy, Inorg. Chem. 47 (2008) 7874-7879.

[63] J. Ihli, W. C. Wong, E. H. Noel, Y-Y. Kim, A. N. Kulak, H K. Christenson, M. J. Duer, F. C. Meldrum, Dehydration and crystallization of amorphous calcium carbonate in solution and in air, *Nature Commun.* **5 (**2014) 3169.

[64] F. M. Michel, J. MacDonald, J. Feng, B. L. Phillips, L. Ehm, C. Tarabrella, J. B. Parise, R. J. Reeder, Structural characteristics of synthetic amorphous calcium carbonate, Chem. Mater. 20 (2008) 4720–4728.

[65] H. Kono, Two-dimensional magic angle spinning NMR investigation of naturally occurring chitins: Precise ^{1}H and ^{13}C resonance assignment of α- and β-chitin, Biopolymers 75 (2004) 255–263.

[66] F. Nudelman, Nacre biomineralisation: A review on the mechanisms of crystal nucleation, Seminars in Cell & Developmental Biology 46 (2015) 2–10.

SUPPLEMENTARY INFORMATION

Structural description of surfaces and interfaces in biominerals by DNP SENS

Thierry Azaïs[a]*, Stanislas Von Euw,[a] Widad Ajili,[a] Stéphanie Auzoux-Bordenave,[b] Philippe Bertani,[c] David Gajan,[d] Lyndon Emsley,[e] Nadine Nassif[a] and Anne Lesage[d]

[a] *Sorbonne Universités, CNRS, Collège de France, Laboratoire Chimie de la Matière Condensée de Paris (LCMCP), 4 place Jussieu F-75005 Paris, France*

[b] *Sorbonne Université, UMR BOREA, Biologie des Organismes et Ecosystèmes Aquatiques, MNHN/CNRS-7208/IRD-207/UPMC, Muséum National d'Histoire Naturelle, Station Marine de Concarneau, Place de la Croix 29900 Concarneau.*

[c] *Laboratoire de RMN et Biophysique des Membranes, UMR 7177 Chimie Université de Strasbourg, Institut Le Bel, 4 rue Blaise Pascal, 67008 Strasbourg*

[d] *High Field NMR Center of Lyon, CRNS/ENS Lyon/ UCB Lyon, 5 rue de la Doua, 69100 Villeurbanne, France*

[e] *Institut des Sciences et Ingénierie Chimiques, Ecole Polytechnique Fédérale de Lausanne (EPFL), CH-1015 Lausanne, Switzerland [d] Strasbourg*

** corresponding author : thierry.azais@upmc.fr*

Figure S1.

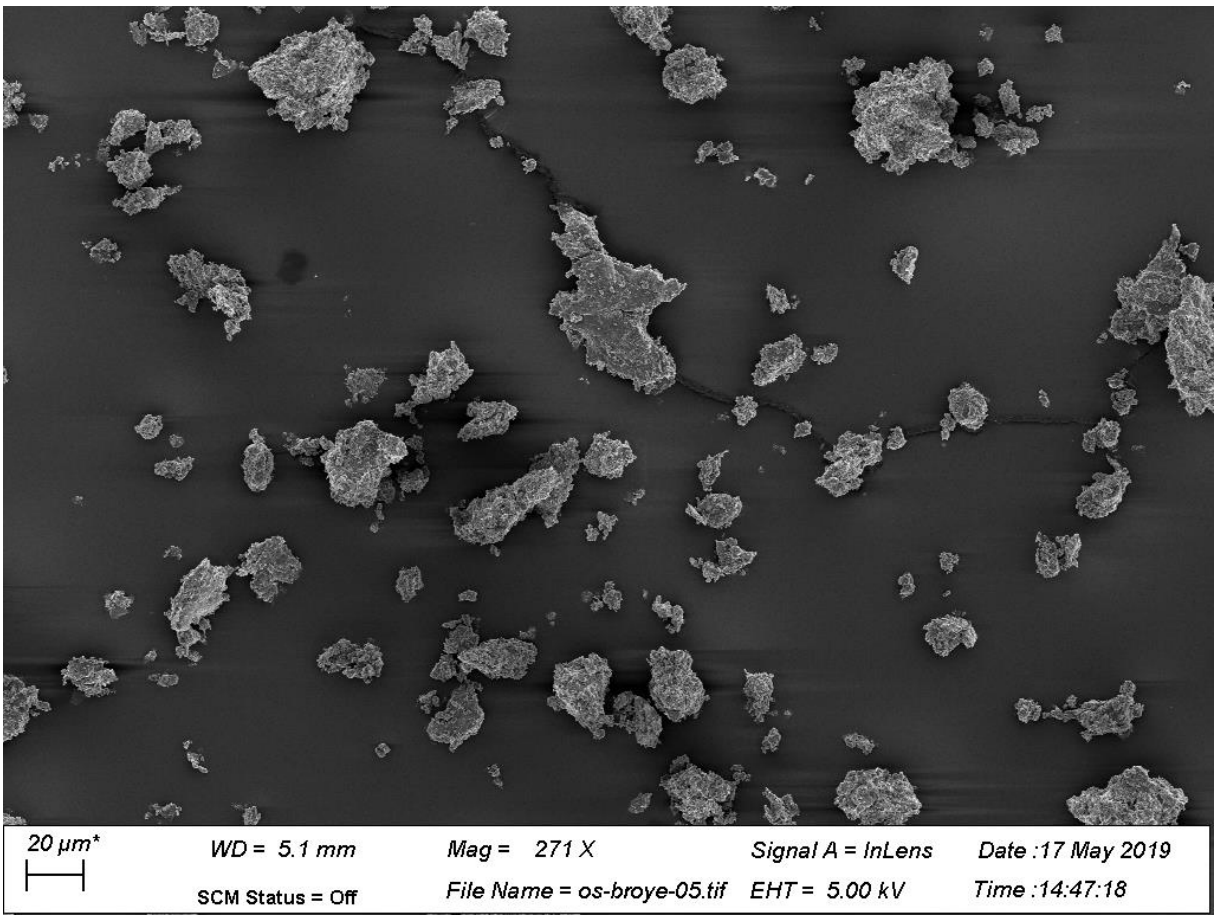

Figure S1: Typical SEM image of crushed bone sample.

Figure S2.

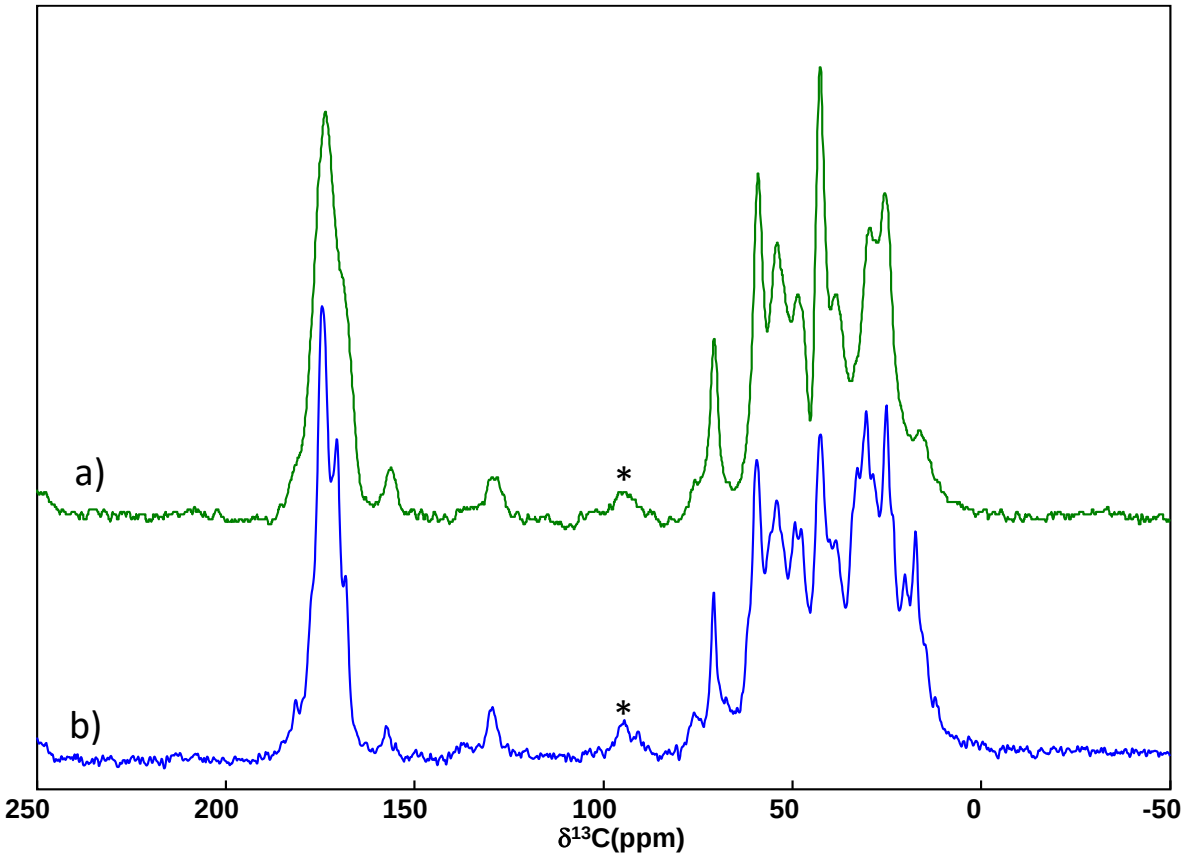

*Figure S2 : ^{13}C CP MAS spectrum of fresh cortical bone recorded through a) DNP MAS conditions (B_0 = 9.4 T; RD = 2 s; t_{CP} = 500 µs, T = 100 K, DNP-impregnation solution without glycerol. Total acquisition time: 4 min) and b) standard MAS conditions (B_0 = 7 T; RD = 1.5 s; t_{CP} = 1 ms, T_{amb}). Total acquisition time: 15h30min). * denotes spinning side-bands.*

Figure S3

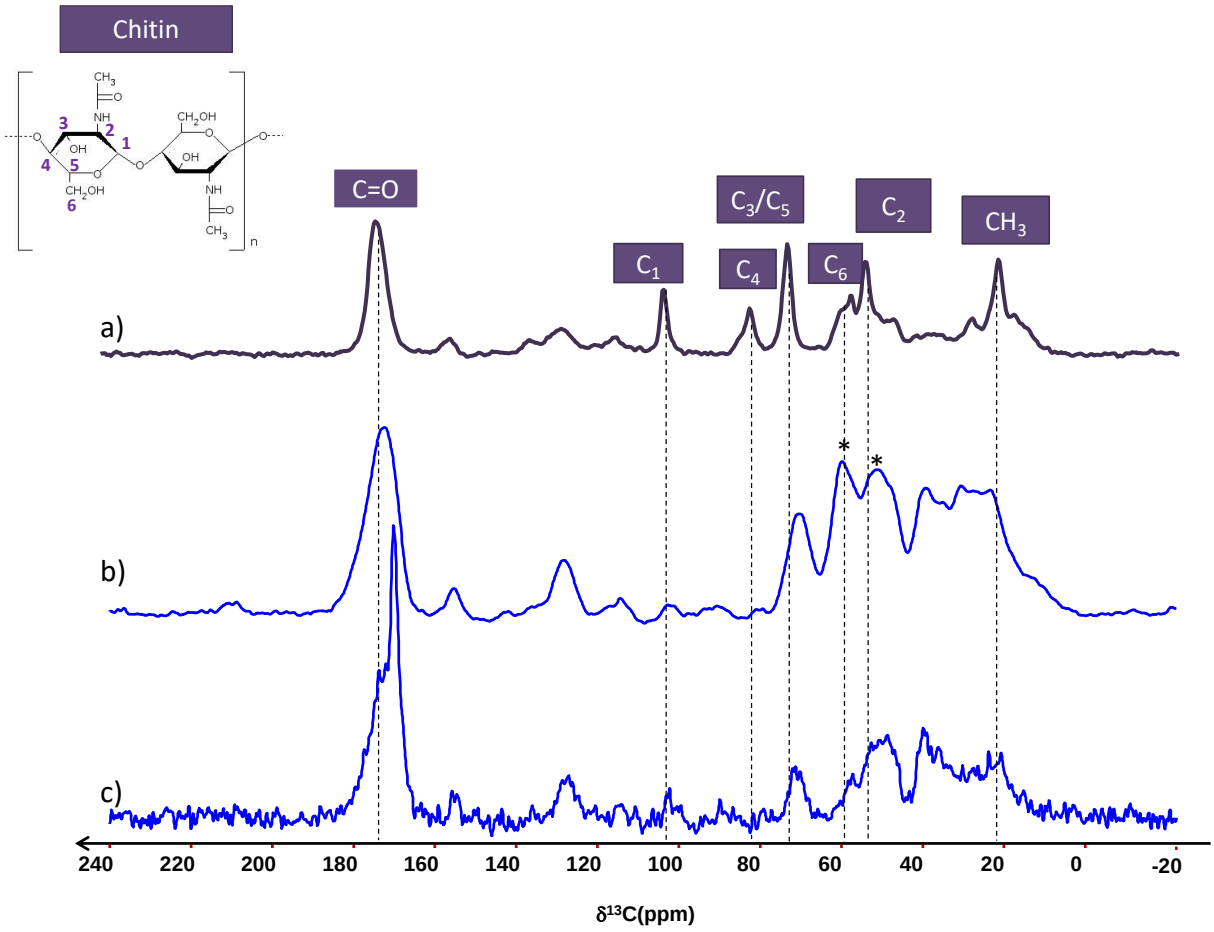

Figure S3: a) ^{13}C CP MAS spectrum of chitin (standard MAS conditions: B_0 = 7 ; t_{CP} = 1 ms, T_{amb}). Chitin resonances are highlighted with dashed lines. b) and c) ^{1}H-^{13}C DNP SENS CP MAS spectra of European abalone shell recorded in the following conditions : b) t_{CP} = 1 ms, DNP-impregnation solution with glycerol (denotes glycerol resonance); c) t_{CP} = 10 ms, DNP-impregnation solution without glycerol.*

Figure S4

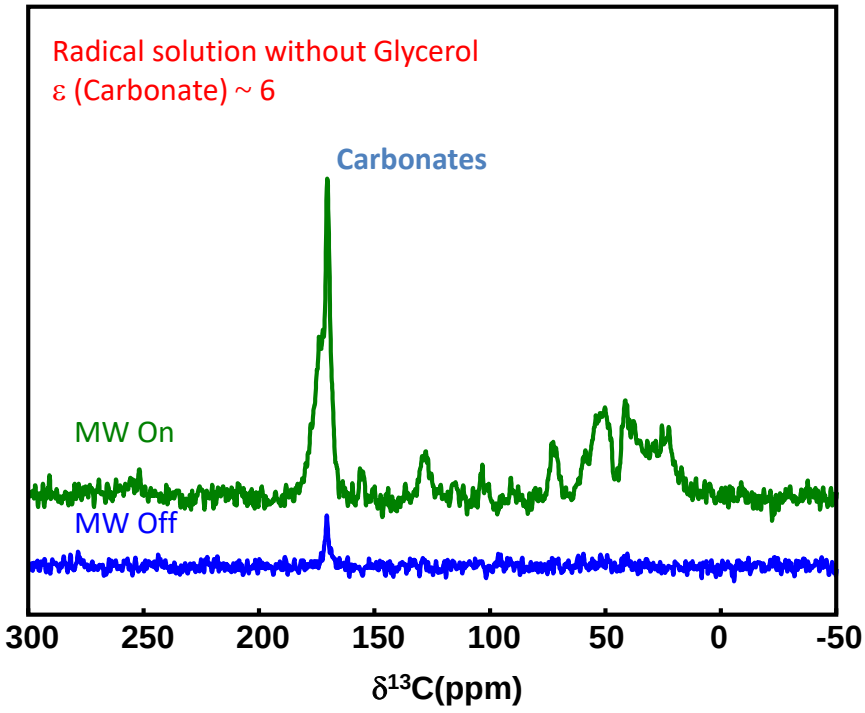

Figure S4: ^{1}H-^{13}C DNP SENS CP MAS spectra of European abalone shell recorded through DNP-impregnation solution without glycerol (t_{CP} = 10 ms; 64 scans).